A Study for Inverse Estimation of Output Strength and Flow Visualization of Burning Rate in the Zr-Ni Type Alloy Delay Compositions

Yang-Hsiung Ko

Department of Power Vehicle and Systems Engineering, CCIT, National Defense University

ABSTRACT

This study presents an on-line inverse method based on the input estimation method formed with both the Kalman filter and the adaptive weighted recursive least squares estimator to estimate the unknown time-varying heat flux at the end of the Zr-Ni type alloy delay compositions (BaCrO4/KClO4/(Zr-Ni)(alloys): 60/14/9(70-30)/17(30-70)) from the transient temperature curve measured using a fine gage thermocouple on the rear of a thin copper disk. The Kalman filter can inversely estimate the unknown heat source strength using the measured temperature on the outer surface, thereby avoiding the divergent problem. The recursive least squares estimator uses the residual innovation sequence from the filter to recursively compute the magnitude of the unknown time-varying heat flux. The results show that this input estimation method structured using the on-line recursive calculation can estimate the unknown time-varying heat flux stably and accurately in inverse heat conduction problems in real time. The research is also based on experimental method to construct a delay-performance-measuring facility by using the flow visualization technique. We discuss the characteristics of flame propagation along with time. The results can be used to optimize the delay device in gun of current army and the control of interior ballistic performance.

Keywords: input estimation method, heat flux, delay compositions

鋯鎳合金系延期藥輸出強度逆向估算及燃速視流化之研究

葛揚雄

國防大學理工學院動力及系統工程學系

摘　　要

本文利用細式熱電偶量測鋯鎳合金系延期藥（鉻酸鋇/過氯酸鉀/鋯-鎳（70/30）/鋯-鎳（30/70）：60/14/9/17）末端輸出強度熱源作用在薄銅片上之背面暫態溫度曲線，再藉由卡爾曼濾波器（Kalman filter）及適應性權重遞迴式最小平方估測器兩者組成之輸入估測法，針對鋯鎳合金系延期藥末端輸出強度之未知時變熱通量進行線上逆向估算。卡爾曼濾波器藉由薄銅片背面之量測溫度，可逆向估算作用在薄銅片正面上之未知熱源強度並避免發散問題；遞迴式最小平方估測器則藉由濾波器產生之剩餘值更新序列遞迴地計算輸入系統之鋯鎳合金系延期藥末端未知時變熱通量。由實驗及逆向估算結果進行分析探討，顯示建立在線上遞迴式計算結構上之輸入估測法，可穩固、精確及即時地估算出逆向熱傳導問題中之延期藥輸出強度。本文亦以實驗方法研究並運用視流技術建構鋯鎳合金系延期藥性能量測實驗設備，探討火焰傳播隨時間變化的影響，可作為改良國軍現行使用火砲延期裝置及內彈道性能控制之參考。

關鍵詞：輸入估算法，熱通量，延期藥

文稿收件日期 101.3.9;文稿修正後接受日期 101.7.18; *通訊作者
Manuscript received Feb 9, 2012; revised July 18, 2012; * Corresponding author

Ⅰ. INTRODUCTION

Many tactical situations call for the introduction of a time delay between an input stimulus and firing. A variety of mechanical and electrical devices has been employed to delay the firing of explosive materiel. However, we are concerned here with the prolongation of the burning phase to provide this delay. Burning forms an important part of the growth of detonation. Hence, it is one of the simplest means for providing delay. It is usually desirable to interpose a column of a special delay material in which the rate of burning is more readily controlled than in material predisposed to the growth of explosion. Since burning rates are affected by such conditions as pressure and temperature and their gradients, it is necessary to take these effects into consideration when designing initiators for delay columns and selecting inert components in which they are housed. In its barest essentials, a delay element is a metal tube with an initiator at one end, a delay column in the middle, and a relay or other output charge at the other end. In addition, depending upon the application and the delay material used, the element may include baffles, igniter mixes at one or both ends of the delay, a housing, and provision for internal free volume. Ignition of one charge by another may be delayed by control of the heat transfer process. Since the burning of gas producing materials depends upon the transfer of heat between the gaseous reaction products and the solid, the burning rate is a direct function of pressure. Thus, the delay times of such delays are greatly influenced by all factors that affect the gas pressure at the burning surface. The burning surface, of course, is all of the surface exposed to the gas, including that of pores and cracks that the gas may penetrate. Reproducible behavior of any delay requires that it burn as a continuous homogeneous substance. Porosity can result in a discontinuous relationship between interface pressure and burning rate. As a gas producing delay burns, the surface in frictional contact with the walls diminishes. The effect of moisture on the burning rate of delay composition is quite complex. For this reason, delay elements must be kept dry. Effects of temperature extremes on performance of delay elements vary appreciably from one delay to another. The spread of data almost invariably increases at extreme temperatures. It may be suspected that these variations are related to subtle design details. The burning rate and the length of delay composition determine the delay time. Even though the chemical delay composition is more inaccurate than the electronic or mechanical delay device, it is still widely used for its simple structure, convenient manufacture and inexpensive cost. The gasless delay compositions are preferred for most applications.

In an obturated system, the pressure in the enclosed free volume is increased, quickly at first, by the primer or flash charge and then progressively by the gas liberated by the burning of the delay column. The result is that the burning rate accelerates continuously. The burning rate does not increase directly with the column length unless the free volume is also increased. This requirement for a volume more or less proportional to the delay time limits

obturated gas producing delays to about 0.4 sec with the common diameter columns of 0.254 to 0.3175 cm. The delay time of an obturated delay element, in addition to its direct relationship to the free volume, is inversely related to the gas volume and heat of explosion of the primer. If the pressure rise in an obturated system is sufficient to cause bursting or significant leakage, the overall burning time will be greatly increased or the delay charge may not sustain its burning.

The gasless delay composition is a mixture of oxidant, fuel and binder. Its burning rate is mainly affected by the type of fuel and the most common used fuel is metal powder. Gasless delay compositions can be classified as fast-propagation (zirconium type), medium-propagation (zirconium-nickel (Zr-Ni) type) and slow-propagation (tungsten type) delay compositions according to their burning rates and metal fuel types [1]. The alloy delay composition is usually a mixture of two metal powders that can be processed to be a cylindrical pellet, long stick or fine wire. The alloy delay composition can be ignited by the ignition system and then its alloy reaction can release sufficient heat to support a burning situation until the delay composition is entirely burned, which has a steady burning rate to provide an accurate delay time.

The purpose of this study is to search the burning properties of Zr-Ni type alloy delay compositions. Many researches of alloy delay compositions [2-5] referred only to the self-propagating high-temperature synthesis technique, and did not touch upon the combustion phenomenon. In this study, the output strength and the burning rate of Zr-Ni type alloy delay compositions are measured using experimental methods.

Substantial theories of the inverse heat conduction problems have been developed and applied in recent years in the heat transfer field [6-11]. Meng [12] presented a modified input estimation method for tracking a maneuvering target. Scarpa and Milano [13] applied the Kalman smoothing technique in inverse heat transfer estimation and accurate results were obtained. Polat [14] used the wall function [15] and the corrected presentation of the shearing stress to explain the influences on material conduction on impact surfaces. Linton and Agonafer [16] utilized the software applied to calculate the fluid dynamic problems to explore the heat-conducting phenomenon on a flat type plate. They compared the simulated results with results from actual experiments. Sathe [17] made use of the numerical simulation method to investigate the flow field and heat transfer by conduction on vertical square-column fins under the impact-emitting flow cooling process. Jonsson and Palm [18] found that the heat resistance value was estimated using the empirical formula from the actual experiment. Maveety and Jung [19] used several flow fields with different Reynolds number values to conduct numerical simulations and compare the results with experimental results.

Heat transfer of a delay element needs to be solved using the system integration approach to deal with the problems produced during the packing, and explosive train manufacturing processes. The amount of heat coming along with delay combustion will expand. The output

strength of temperature can be estimated when the time-varying heat flux produced by the alloy delay compositions can be sufficiently measured in real time. This study proposes input estimation method to estimate the unknown time-varying heat flux inversely using the measured temperature at the rear of a thin copper disk. Additionally, the distribution of the estimated temperature curve can be obtained accurately.

The military first applied the input estimation method [20] to the target tracking problem. A sliding window was used to accumulate the residuals produced by the Kalman filter, adopting the generalized least squares method to estimate the unknown definite acceleration input value. The whole batch processing method with time consuming calculations was used. The input estimation method based on the Kalman filter and the recursive least squares estimation method was used to resolve the calculation problem. The unknown time-varying variables were estimated in real time, powerfully reducing the computational processes. The Kalman filter is used to produce a residual renewal array. The recursive least squares method applies the renewal array to compute the uncertainties recursively. This information provides useful suggestions for thermal processing in military explosive design.

Ⅱ. ANALYSIS

This study applies input estimation method to estimate the inner delay heat source inversely with the rear temperature field in a thin copper disk. The temperature is measured using the K-type fine gage thermocouples. The copper disk is thin enough to assume that it is a homogeneous thermal conductor with thickness L. A free convection h boundary condition exists at the position $x=L$. The time-varying heat flux $q(t)$ produced from the Zr-Ni type alloy delay compositions is at position $x=0$. The K-type fine gage thermocouple is welded onto the center rear of a thin copper disk at position $x=L$ to measure the rear surface temperature. A diagram of the heat transfer model is shown in Fig.1.

Assumptions: 1. Steady-state conditions. 2. One-dimensional conduction in x. 3. Constant properties. 4. No internal heat generation. 5. Negligible radiation exchange with surroundings. 6. Uniform convection coefficient over outer surface.

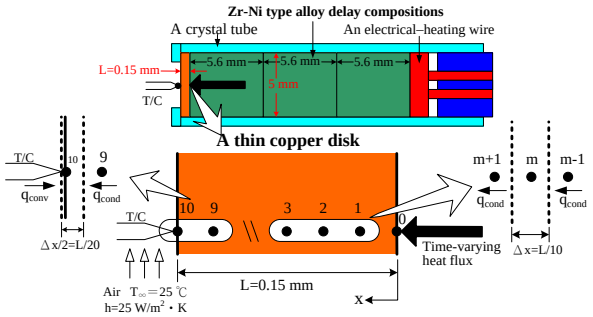

Fig. 1. Physical model of one dimensional inverse heat conduction problem (geometry and coordinates).

The governing equations for heat conduction are as follows:

$$\frac{\partial}{\partial x}\left(k_{co}\frac{\partial T(x,t)}{\partial x}\right)=\rho c_p\frac{\partial T(x,t)}{\partial t}$$

$$0\le x\le L,\ 0<t\le t_f \qquad (1)$$

To solve (1) for the temperature distribution $T(x,t)$, it is necessary to specify an initial conduction and two boundary conductions. The

initial conduction is

$$T(x,0)=T_i \tag{2}$$

and the boundary conductions are

$$-k_{co}\left.\frac{\partial T}{\partial x}\right|_{x=0}=q''_x \tag{3}$$

and

$$-k_{co}\left.\frac{\partial T}{\partial x}\right|_{x=L}=h\left[T(L,t)-T_\infty\right] \tag{4}$$

where $T(x,t)$ is the temperature function for time t and the position x. T_i is the initial temperature. The proportionality constant k_{co} is a transport property known as the thermal conductivity $(W/m\cdot K)$ of a thin copper disk. Density ρ and specific heat c_p are two such properties used extensively in thermodynamic analysis. The product ρc_p $(J/m^3\cdot K)$, commonly termed the volumetric heat capacity, measures the ability of a material to store thermal energy.

When a fine gage K-type thermocouple is placed at position $x=L$, the measured temperature $z(t)$ is described as

$$z(t)=T(L,t)+v(t) \quad t>0 \tag{5}$$

$v(t)$ is the measurement noise assumed to be Gaussian white noise with zero mean.

To obtain the finite-difference form of Equation (1), we use the central difference approximations to the spatial derivatives. The subscript i may be used to designate the x location of discrete nodal point. The central differential method in Equation (1) is expressed as

$$\dot{T}_0(t)=\frac{\alpha}{\Delta x^2}\left[-2T_0(t)+2T_1(t)\right]+\frac{2q(t)}{\rho c_p\Delta x} \quad i=0 \tag{6}$$

$$\dot{T}_i(t)=\frac{\alpha}{\Delta x^2}\left[T_{i+1}(t)-2T_i(t)+T_{i-1}(t)\right]$$

$$i=1,2,.....,N-1 \tag{7}$$

where the space interval $\Delta x=L/N$ and $T_i(t)=T(x_i,t)$. In heat transfer analysis, the thermal conductivity ratio to the heat capacity is an important property term in thermal diffusivity $\alpha=k_{co}/\rho c_p$, which has units of m^2/s. It measures the ability of a material to conduct thermal energy relative to its ability to store thermal energy.

The boundary condition Equation (4) can be expressed as

$$\dot{T}_N=\frac{2\alpha}{\Delta x^2}T_{N-1}-\frac{2\alpha}{\Delta x^2}T_N-\frac{2h}{\rho c_p\Delta x}T_N+\frac{2h}{\rho c_p\Delta x}T_\infty \tag{8}$$

The continuous-time state equation can be obtained below along with a simulated noise input:

$$\dot{T}(t)=\Psi T(t)+\Omega q(t)+Gw(t)+Dh \tag{9}$$

where

$$\Psi=\frac{\alpha}{\Delta x^2}\begin{bmatrix} -2 & 2 & 0 & \cdots & \cdots & 0 \\ 1 & -2 & 1 & \ddots & \cdots & 0 \\ 0 & 1 & -2 & 1 & \cdots & \vdots \\ \vdots & \ddots & & \ddots & \cdots & \vdots \\ \vdots & & \ddots & 1 & -2 & 1 \\ 0 & \cdots & \cdots & \cdots & 2 & -2-\frac{2h\Delta x}{k_\infty} \end{bmatrix} \tag{10}$$

$$T(t)=\left[T_0(t)\ \ T_1(t).....T_{N-1}(t)\ \ T_N(t)\right]^T \tag{11}$$

$$\Omega=\left[\frac{2}{\rho c_p\Delta x}\ \ 0.....0\ \ 0\right]^T \tag{12}$$

$$D=\begin{bmatrix} 0 \\ 0 \\ \vdots \\ \vdots \\ \frac{2T_\infty}{\rho c_p\Delta x} \end{bmatrix} \tag{13}$$

w(t) is assumed to be Gaussian white noise with zero mean and represents the modeling error.

However, the problem must be descretized in time in addition to space. Equation (7), the continuous-time state equation, can be discretized with the sampling timeΔt. The discrete-time state equation may be expressed as

$$T(k+1) = \Phi[(k+1)\Delta t, k\Delta t]T(k) + \Gamma(k+1)q(k) + w(k+1) + \Lambda h \quad (14)$$

and its relative equations are

$$\Phi[(k+1)\Delta t, k\Delta t] = e^{A\Delta t} \quad (15)$$

$$\Gamma(k+1) = \int_{k\Delta t}^{(k+1)\Delta t} \Phi[(k+1)\Delta t, \tau]B(\tau)d\tau \quad (16)$$

$$w(k+1) = \int_{k\Delta t}^{(k+1)\Delta t} \Phi[(k+1)\Delta t, \tau]G(\tau)w(\tau)d\tau \quad (17)$$

$$\Lambda = \int_{k\Delta t}^{(k+1)\Delta t} \Phi\left[(k+1)\Delta t, \tau\right]D(\tau)d\tau \quad (18)$$

where Φ is the state transition matrix. *T(k)* is the state vector.Γ*(k)* is the input matrix. *q(k)* is the definite input array. *w(k)* is the processing error input vector assumed to be Gaussian white noise with zero mean. The variance $E\{w(k)w^T(j)\} = V_{pn}\delta_{kj}$. V_{pn} is the processing error variance. δ_{kj} is the Dirac delta function.

The discrete time measurement equation is expressed as

$$z(k) = HT(k) + v(k) \quad (19)$$

where *z(k)* is the observation vector at the k^{th} sampling time. *H*=[0 0 ….1] is the measurement matrix. *v(k)* is the measurement error vector assumed to be the Gaussian white noise with both zero mean and the variance $E\{v(k)v^T(j)\} = V_{mn}\delta_{kj}$. V_{mn} is the measurement error variance.

After the state equation is obtained, the inverse estimation process is carried out using the input estimation method based on the Kalman filter and the recursive least squares estimation algorithm.

Input Estimation Method

The system input is the unknown time-varying heat flux. The Kalman filter works under the V_{pn} (processing error variance) and the V_{mn} (measurement error variance) settings and makes use of the difference between the measurements and the estimated system temperature values as the functional index. The time-varying heat flux can be accurately predicted using the recursive least squares algorithm. The Kalman filter equations are expressed as

$$\bar{X}\left(k/k-1\right) = \Phi\bar{X}\left(k-1/k-1\right) + \Lambda h \quad (20)$$

$$P(k/k-1) = \Phi P(k-1/k-1)\Phi^T + V_{pn} \quad (21)$$

$$s(k) = HP(k/k-1)H^T + V_{mn} \quad (22)$$

$$K(k) = P(k/k-1)H^T s^{-1}(k) \quad (23)$$

$$P(k/k) = [I - K\left(k\right)H]P(k/k-1) \quad (24)$$

$$\bar{Z}(k) = Z(k) - H\bar{X}(k/k-1) \quad (25)$$

$$\bar{X}(k/k) = \bar{X}(k/k-1) + K(k)\bar{Z}(k) \quad (26)$$

The recursive least squares algorithm equations are expressed as

$$B(k) = H[\Phi M(k-1) + I]\Gamma \tag{27}$$

$$M(k) = [I - K(k)H][\Phi M(k-1) + I] \tag{28}$$

$$K_b(k) = \gamma^{-1} P_b(k-1) B^T(k) \left[B(k)\gamma^{-1} P_b(k-1) B^T(k) + s(k) \right]^{-1} \tag{29}$$

$$P_b(k) = \left[I - K_b(k) B(k) \right] \gamma^{-1} P_b(k-1) \tag{30}$$

$$\hat{q}(k) = q(k-1) + K_b(k) \left[\bar{Z}(k) - B(k)\hat{q}(k-1) \right] \tag{31}$$

$$\hat{X}(k/k-1) = \Phi X(k-1/k-1) + \Gamma \hat{q}(k) + \Lambda h \tag{32}$$

$$\hat{X}(k/k) = X(k/k-1) + K(k) \left[Z(k) - H\hat{X}(k/k-1) \right] \tag{33}$$

where P is the filtering error covariance matrix. $s(k)$ is the residual covariance. $\bar{Z}(k)$ is the bias innovation produced by the measurement noise and the input disturbance. $B(k)$ and $M(k)$ are the sensitivity matrices. $K_b(k)$ is the correction gain. $P_b(k)$ is the error covariance of the estimated input vector.γ is the weighting constant or weighting factor in the range $0 < \gamma \leqq 1$. $\hat{q}(k)$ is the estimated input vector.

Ⅲ. EXPERIMENTAL METHODS

In the time-varying heat flux for the Zr-Ni type alloy delay compositions, the measurement method must cope with rapidly changing burning chiefly with the following temperature measurements (Fig.2). A schematic diagram of the PC-based data acquisition system used for the temperature measurement is shown in Fig. 3.

1. A fine gage thermocouple

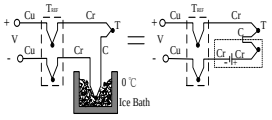

2. Hardware compensation

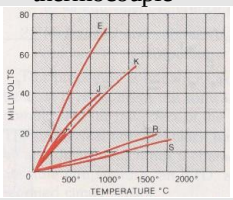

3. ℃ vs. V graph

4. 5B40

5. 5B16B

6. MultiPro 120

7. IEEE-488 interface card

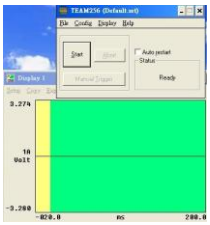

8. Team 256 software

The whole experimental facility

Fig. 2. Temperature measurements.

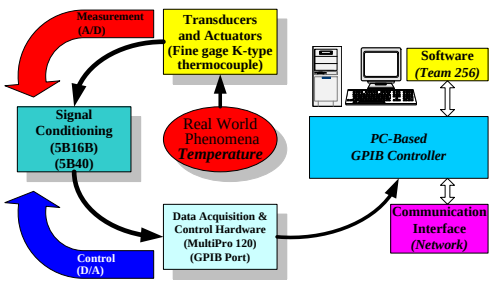

Fig. 3. Schematic diagram of the experimental facility.

3.1 Thermocouples

One of the most frequently used temperature sensors is the thermocouple. Thermocouples are inexpensive temperature sensing devices widely used with PC-based data acquisition (DAQ) systems. Thermocouples are very rugged, inexpensive devices that operate over a wide temperature range. A thermocouple is created whenever two dissimilar metals touch and the contact point produces a small open-circuit voltage as a function of temperature. The voltage is nonlinear with respect to temperature. However, for small changes in temperature, the voltage is approximately linear. The K-type fine gage thermocouple (Fig.2-1) has one nickel-chromium alloy conductor and one nickel-aluminum alloy conductor. Thermocouples require some form of temperature reference to compensate for these unwanted parasitic cold junctions. The most common method is to measure the temperature at the reference junction with a direct-reading temperature sensor and subtract the parasitic junction voltage contributions. This process is called cold-junction compensation. By using the thermocouple law of intermediate metals and making some simple assumptions, the voltage of a DAQ system measures depends only on the thermocouple type, the thermocouple voltage, and the cold-junction temperature. The measured voltage is in fact independent of the composition of the measurement leads and the cold junctions. There are two techniques for implementing cold-junction compensation: hardware compensation and software compensation. Both techniques require that the temperature at the reference junction be sensed with a direct-reading sensor. A direct-reading sensor has an output that depends only on the temperature of the measurement point. With hardware compensation (Fig.2-2), a variable voltage source is inserted into the circuit to cancel the parasitic thermoelectric voltages. The variable voltage source generates a compensation voltage according to the ambient temperature, and thus adds the correct voltage to cancel the unwanted thermoelectric signals. When these parasitic signals are canceled, the only signal of a data acquisition system measures is the voltage from the thermocouple junction.

We used K-type fine gage thermocouples whenever fast, accurate temperature measurements were required. The fine wire diameters enable accurate temperature measurements without disturbing the base temperature of the body by keeping heat transfer via the leads to a minimum. They are available in wire sized 0.125 mm in diameter. To insure consistent thermoelectric properties, the fine gage thermocouples are made from carefully selected materials, made from matched wire pairs within the same lot number.

Thermocouple output voltages are highly nonlinear (Fig.2-3). For this reason, we must either approximate the thermocouple voltage-versus-temperature curve using the polynomial or use a look-up table. The polynomial of K-type thermocouple voltage (V)-to-temperature (℃) conversion is in the following form:

$$T=a_0+a_1x+a_2x^2+a_3x^3+a_4x^4+a_5x^5+a_6x^6+a_7x^7+a_8x^8$$

where

T= Temperature in ℃, x= Thermocouple voltage in V, a_0=0.226584602, a_1=24152.109,

a_2= 67233.4248, a_3= 2210340.682,
a_4= -860963914.9, a_5=4.83506×10^{10},
a_6=-1.18452×10^{12}, a_7= 1.38690×10^{13},
a_8= -6.33708×10^{13}.

3.2 Signal Conditioning-5B Series Modules

The signals of thermocouple output are typically in the mV range, making them susceptible to noise. Lowpass filters are commonly used in thermocouple DAQ systems to effectively eliminate high frequency noise in thermocouple measurements. We improve the noise performance of the system by amplifying the low-level thermocouple voltages near the signal source. Because thermocouple output voltage levels are very low, we choose a gain that optimizes the input limits of the analog-to-digital converter. Another source of noise is due to thermocouples being soldered directly to a slice of copper. This configuration makes thermocouples particularly susceptible to common-mode noise and ground loops. Isolation helps to prevent ground loops from occurring, and can dramatically improve the rejection of common-mode noise. With conductive material that has a large common-mode voltage, isolation is required as non-isolated amplifiers cannot measure signals with large common-mode voltages.

Thermocouples generate signals too small to measure directly with a DAQ device. When dealing with small voltages, noisy environments, extreme low signals, or simultaneous signal measurement, signal conditioning is essential for an effective DAQ system. Signal conditioning maximizes the accuracy of a system, allows sensors to operate properly, and guarantees safety. It is important to select the right hardware for signal conditioning. Signal conditioning is offered in modular.

The 5B40 wide bandwidth voltage input module (Fig.2-4) provides a single channel of analog input which is amplified, isolated and converted into high-level analog voltage output. This voltage output is logic-switch controlled, allowing these modules to share a common analog bus without the need for external multiplexers. The input signal is processed through a pre-amplifier on the field side of the isolation barrier. This pre-amplifier has a gain-bandwidth product of 5MHz and is bandwidth limited to 10 kHz. After amplification, the input signal is chopped by a proprietary chopper circuit. Isolation is provided by a transformer coupling, again using a proprietary technique to suppress common mode spike or surge transmission. This module is powered from +5VDC, ±5%.

The 5B16B 16-channel back panel (Fig.2-5) which has 16 non-addressable analog I/O signal channels and includes on-board temperature sensors and cold junction compensation (CJC), power supplies, mounting racks, interface cables and evaluation boards, accepts the 5B analog modules in any mixture.

3.3 High-speed DAQ Hardware

Nicolet MultiPro 120 (MP) (Fig.2-6) acts as the interface between the computer and the outside world. It functions primarily as a device that digitizes incoming analog signals so that the computer can interpret them. Its functions include a combination of analog, digital and counter operations on a single device for powerful transient measurement.

MP complies with the IEEE-488.2 standard for convenient interface (Fig.2-7) with GPIB instruments. Without software to control or drive the MP, the MP will not work properly. The driver software of 488.2 transforms the PC and the MP into a complete data acquisition, analysis and presentation tool. It is the layer of software that permits easy communication with the MP and has no need for register-level programming or complicated commands to access the MP functions. It forms the middle layer between the application software and the MP.

The application software of Team 256 (Fig.2-8) adds analysis and presentation capabilities to the driver software. Team 256 is an easy-to-use yet very flexible tool specifically designed for data logging applications. With intuitive dialog windows, it can configure our logging task to easily acquire, log, view and share data. It is a stand-alone and configuration-based data logging software.

3.4 Ignition System

The ignition system (Fig.4) is composed of an electrical–heating wire, a transformer, and a timekeeper. A column of delay composition is usually preceded by the ignition system. Electrical–heating wires are necessary when the delay compositions are insensitive to be initiated directly by the agent used in the particular application.

Fig. 4. An ignition system.

3.5 Investigation of Burning Rate

For investigating combustion, the Kodak Ektapro hi-spec motion analyzer (Fig.5) is used to record burning events and provide immediate, slow-motion playback. The system is ideal for use in ballistic testing on ranges and high-speed

（Kodak EktaPro Hi-Spec Processor）

（Kodak EktaPro Hi-Spec Keypad and Imager）

Fig. 5. The Kodak Ektapro hi-spec motion analyzer.

events with its rugged design and ability to capture up to 12000 pictures per second. The live setup feature allows us to be sure that the image is exactly what is required to solve the problem. Owing to the large number of frames per second, the motion is truly reproduced. The high rate of frames is attained by replacing the usual intermittent motion of the slide tray (processor memory, Fig.6) by a continuous one and by optical phasing. The slide tray is moved around and wound up by separate electromotors. Its speed (and the number of frames/sec) is controlled by varying the voltage of the motors. With a rate of 1000 frames per second, the Kodak EktaPro hi-spec motion analyzer is a system used to record burning flamespreading events of the delay compositions.

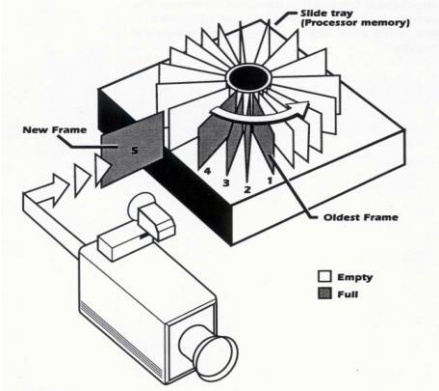

Fig. 6. Slide tray (processor memory).

3.6 Zr-Ni Type Alloy Delay Compositions

The formulas of the alloy delay compositions are variations of a standard formula with a weight % of $BaCrO_4$/$KClO_4$/(Zr-Ni)(alloys): 60/14/9(70-30)/17(30-70). The formulations of delay compositions are shown in Table 1. The Zr-Ni type alloy delay compositions are processed to be delay columns. There are several steps to prepare the delay columns: drying of the ingredients, precise weighing, premixing of the ingredients, first screening, mechanical mixing, second screening, adding of solvent and binder, pelleting, screening and selecting, final drying. The length of a delay column is 5.6 mm with a diameter of 5 mm.

Table 1. The formula of Zr-Ni type alloy delay compositions

Composition				Approximate Inverse Burning Rate
$BaCrO_4$	$KClO_4$	(Zr-Ni) (alloys) (70-30)	(Zr-Ni) (alloys) (30-70)	Sec/cm
60	14	9	17	2.3

Ⅳ. RESULTS AND DISCUSSIONS

The delay column supplemented by one or more delay charges is means by which the burning of the propelling mixture is initiated. The delay compositions contain the Zr-Ni type alloy mixtures designed to be sensitive to shock, mechanical or electrical, in accordance with the means of firing provided by the gun. On activation by the ignition system, the delay composition projects a hot flame. The combustion characteristics of the delay compositions depend on a number of factors such as temperature, pressure, particle size, compact density, heat output, and thermal conductance. The Zr-Ni type alloy delay compositions are processed to be delay columns loaded in the crystal tube(Fig.7). The minimum

Fig. 7. Three delay columns loaded in the crystal tube.

ignition energy, burning rate, and output strength are measured by means of experimental apparatuses to investigate the relationships between the delay composition and the thermal conductance of copper during the delay burning. The experimental results can be applied as design guidelines of the control of interior ballistic performance.

This section discusses the voltage vs. time, temperature vs. time, and time-varying heat flux vs. time determination using a K-type fine gage thermocouple. The temperature of a thin copper disk may be measured as a function of time

using the thermocouple. This sensor generates a voltage proportional to the temperature which is applied as the ordinate of the MP. The abscissa is elapsed time.

The measured curves for voltage vs. time and temperature vs. time are shown in Fig.8 (a) and (b) from the rear of the thin copper disk ($x=L$) on the one pellet of delay column charged delay composition. These data are analyzed on-line to estimate the corresponding time-varying heat flux calculated by the input estimation method. Thus time-varying heat flux vs. time (Fig.8 (c)) may be obtained from Fig.8 (b). In order to aid the contrast and judge the estimated time-varying heat flux, direct heat conduction problem is used to solve the estimated temperature curve (Fig.8 (d)) from the time-varying heat flux vs. time data (Fig.8 (c)). The value of RMS between the estimated temperature curve (Fig.8 (d)) and the measured temperature curve (Fig.8 (b)) is 0.075 ℃. Fig.8 (d) is similar to Fig.8 (b). Therefore, it appears that the estimated time-varying heat flux is the heat flux generated by the delay composition on the thin copper disk front.

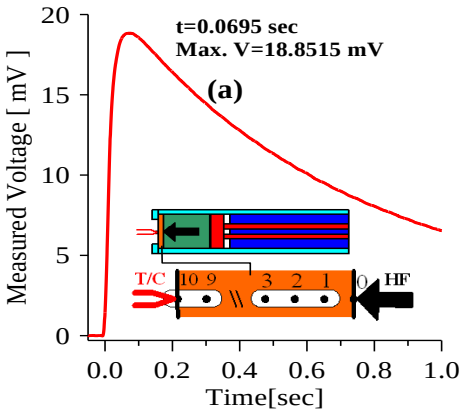

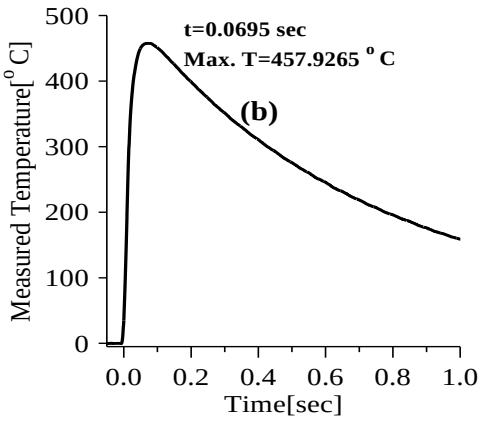

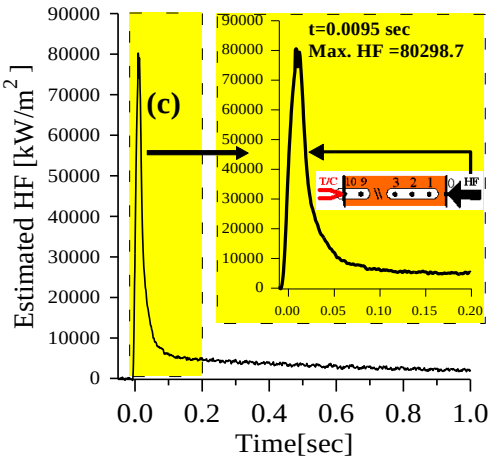

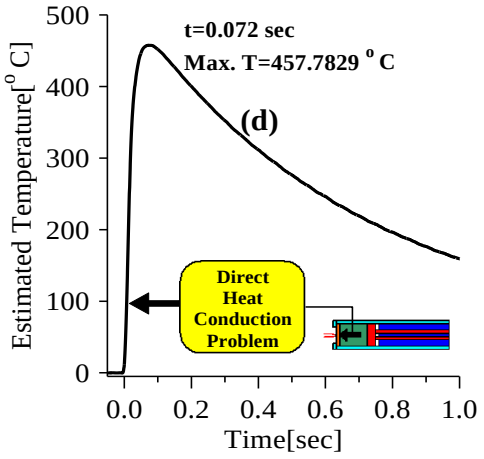

Fig. 8. (a) Voltage-time relationship determined experimentally at $x=L$ from a slice of copper for a properly ignited pellet of delay column. (b) Experimental measured temperature-time curve by V-to-℃ conversion. (c) Estimated time-varying heat flux–time curve at $x=0$ by input estimation method with measured temperature in (b) as input. (d) Estimated temperature-time curve at $x=L$ by direct heat conduction problem with estimated time-varying heat flux in (c) as input.

To illustrate the input estimation method accuracy, we considered two specific experiments involving estimation of the time wise variation in the time-varying heat flux strength located on the thin copper disk front and the transient temperature recording taken on the rear. Comparing the two delay examples (two pellets and three pellets) with Fig.9 (a), it appears that the peak temperature on the thin copper disk rear to two delay pellets at about 0.0535 sec is 468.9957 ℃ and the other at about 0.063 sec is 477.0049 ℃. The RMS values between the estimated temperature curves (Fig.9 (c)) and the measured temperature curves (Fig.9 (a)) are 0.427 ℃ and 0.677 ℃, respectively. Therefore, the prediction and measurement of temperatures (Fig.9 (c) and (a)) are in good agreement. The results show that the input estimation method accuracy is good.

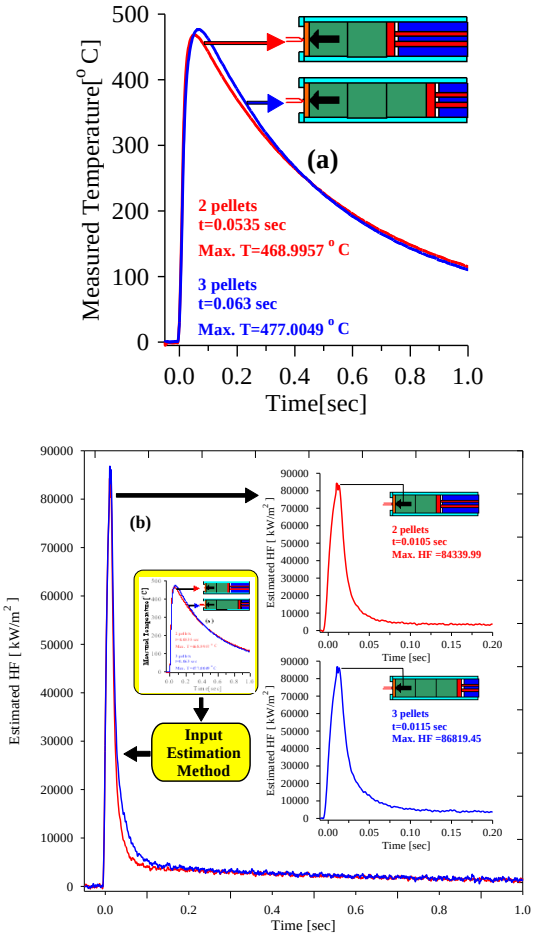

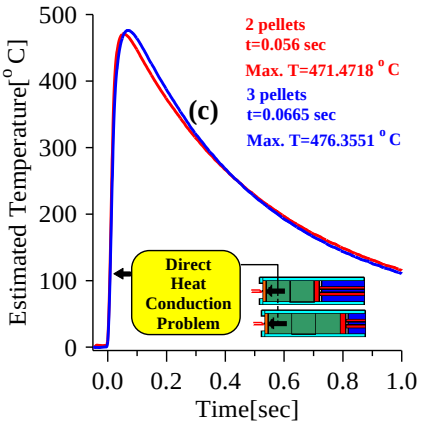

Fig. 9. (a) Experimentally measured temperature-time curves at $x=L$ for properly ignited two pellets and three pellets of delay columns. (b) Estimated time-varying heat flux–time curves at $x=0$ by means of input estimation method with the measured temperatures in (a) as input. (c) Estimated temperature-time curves at $x=L$ by means of direct heat conduction problem with the time-varying heat flux in (b) as input.

Fig.10 shows snap shots of burning propagation by means of Kodak Ektapro hi-spec motion analyzer for three delay columns. According to the experimental results, the minimum ignition energy and burning rate of the Zr-Ni type alloy delay compositions are 80.3328 J and 3.2 mm/sec. The K-type fine gage thermocouple is placed at the end of crystal tube to measure the temperature of output flame. The value of maximum temperature is 572 ℃. The minimum ignition energy measured by means of the ignition system is the minimum energy input required to initiate combustion of the delay composition. Several major regions are present in a delay column. The actual self-propagating exothermic process is occurring in the reaction zone. High temperature, flame and smoke production, and the likely presence of gaseous and liquid materials characterize this region. Behind the advancing reaction zone are solid products formed during the reaction. Immediately ahead of the reaction zone is the next layer of composition that will undergo

reaction. This layer is being heated by the approaching reaction, and melting, solid-solid phase transitions, and low-velocity pre-ignition reactions may be occurring. The thermal conductivity of the composition is quite important in transferring heat from the reaction zone to the adjacent, unreacted material. Hot gases as well as hot solid and liquid particles aid in the propagation of burning.

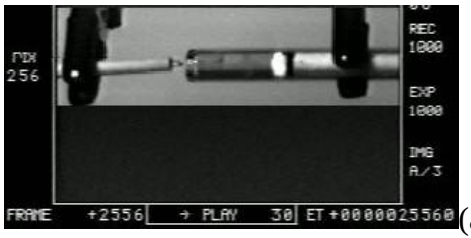

(a)

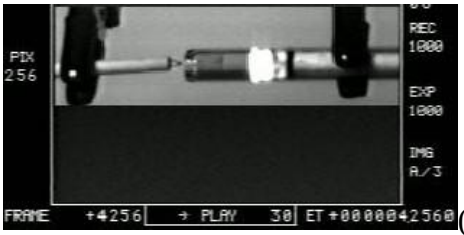

(b)

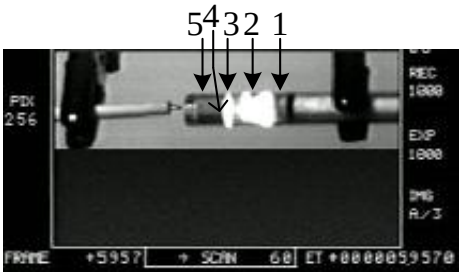

(c)

1. Ignition stimulus applied here
2. Reaction products (Residue)
3. Reaction zone (Flame)
4. Adjacent layer being heated as reaction zone nears
5. Unreacted material

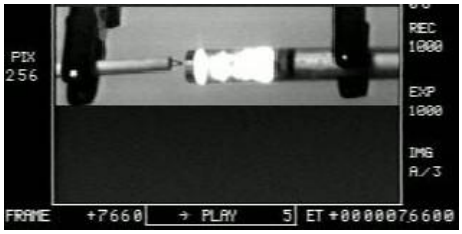

(d)

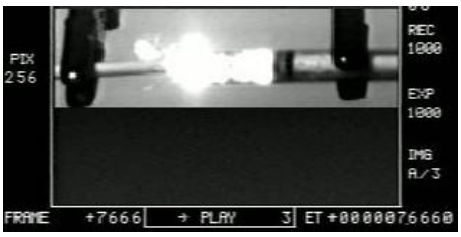

(e)

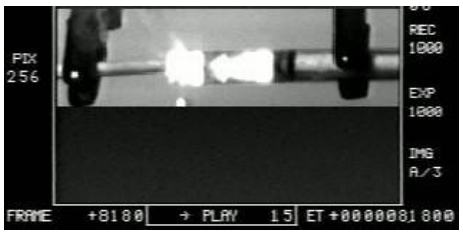

(f)

Fig. 10. The snap shots of combustion propagation by means of Kodak Ektapro hi-spec motion analyzer for three pellets of delay columns loaded in the crystal tube. (a) The first pellet of delay column is ignited. (b) The second pellet of delay column is ignited. (c) The third pellet of delay column is ignited. (d) The third pellet of delay column burns at the extreme end. (e) The output of combustion flame is violent. (f) The output of combustion flame weakens.

V. CONCLUSIONS

This study shows that the input estimation method, including the extended Kalman filter and on-line input estimation, can accurately and efficiently estimate the time-varying heat flux inside delay compositions in real time and produce a rapid reaction speed when the length of the sampling time is short. The proposed method has the superior capability to perform unknown heat source estimation and accurately compute the temperature distribution of inverse heat conduction problem. In contrast to an off-line or batch-form approach, the recursive mode structure reduces the calculation load such that measurement of the whole batch of temperature data is not necessary. The transient temperature measurement method is presented in this work as well. The applications are valuable in work efficiency and the immediate

identification of unknowns such as the super-quick heat flux or the impulse heat sources in explosives. The burning rates of Zr-Ni type alloy delay compositions are measured using experimental methods. A Kodak Ektapro hi-spec motion analyzer is used to record the combustion phenomena such as ignition and flame propagation. Additionally, the output strength is estimated by the input estimation method. The effects of alloy delay compositions on the ignition, burning rate, and output strength are evaluated from experimental data. The results are useful for the optimal design of delay device in gun of current army and the control of interior ballistic performance.

REFERENCES

[1] U. S. Army, Military explosives, TM9-1300-214, Department of the Army, Technical Manua, Washington, pp. 8–32, 1984.

[2] Burke, A. R., Brown, C. R., Bowling, W. C., Glaub, J. E., Kapsch, D., Love, C. M., Whitaker, R. B., and Moddeman, W. E. "Surface and Interface Analysis," Vol. 11, Issue 6-7, pp. 353–358, April 1988.

[3] Ma, Z. Y., Tjong, S. C., and Gen, L. "In-situ Ti-TiB metal matrix composite prepared by a reactive pressing process," Scripta Materialia, Vol. 42, pp. 367–373, 2000.

[4] Li, D. X., Ping, D. H., Lu, Y. X., and Ye, H. Q., "Characterization of the microstructure in TiB whisker reinforced titanium alloy matrix composite," Mater Letters, Vol. 16, No. 6, pp. 322–326, 1993.

[5] Tsuchida, T. and Yamamoto, S., "The SEM microphotographs of the particles of Zr, B and C," Journal of the European Ceramic Society, Vol. 24, pp. 45–51, 2004.

[6] Woo, K. C. and Chow, L. C., "Inverse Heat Condition by Direct Inverse Laplace Transform," Numerical Heat Transfer, Vol.4, pp.499-504, 1981.

[7] Jarny, Y., Ozisik, M. N., and Bardon, J. P., "A General Optimization Method Using Adjoint Equation for Solving Multidimensional Inverse Heat Conduction," Int. J. Heat Mass Transfer, Vol. 34, pp. 2911-2919, 1991.

[8] Huang, C. H. and Ozisik, M. N., "Inverse Problem of Determining the Unknown Strength of an Internal Plane Heat Source," J. Franklin Institute Pergamon Press Ltd, Vol.329, No. 4, pp. 751-764, 1992.

[9] Silva Neto, A. J. and Ozisik, M. V., "Simultaneous Estimation of Location and Timewise-Varying Strength of a Plane Heat Source," Numerical Heat Transfer, Part A, Vol. 24, pp. 467-477, 1993.

[10] Kalman, R. E., "A New Approach to Linear Filtering to the Calibration and Alignment of Inertial Navigation Systems," ASME J. Basic Eng., series 82d, pp. 35-45, 1960.

[11] Chan, Y. T., Hu, A. G. C., and Plant, J. B., "A Kalman Filter Based Tracking Scheme with Input Estimation," IEEE Transactions on Aerospace and Electronic Systems, ASE-15, pp. 237-244, 1979.

[12] Meng, H. H., Aircraft Maneuver Detection Using an Adaptive Kalman Filter, Master's Thesis, Naval Postgraduate School, Monterey, California, USA.

[13] Scarpa, F. and Milano, G., "Kalman Smoothing Technique Applied to the Inverse Heat Conduction Problem," Numerical Heat Transfer. Part B, Vol. 28,

pp. 79-96, 1995.

[14] Polat, S., Mujumdar, A. S., Heiningen, A. R. P., and Douglas, W. J. M., "Numerical Model for Turbulent Jet Impinging on a Surface with Through-Flow," Int. J. Thermophysics, Vol. 5, No. 2, pp. 172-180, 1991.

[15] Chieng, C. C. and Launder, B. E., "On the Calculation of Turbulent Heat Transport Downstream from an Abrupt Pipe Expansion," Numerical Heat Transfer, Vol. 3, pp. 189-207, 1980.

[16] Linton, R. L. and Agonafer, D., "Coarse and Detailed CFD Modeling of a Finned Heat Sink," IEEE Transactions on Components Packaging and Manufacturing Technology A, Vol. 18, No. 3, pp. 517-520, 1995.

[17] Sathe, S., Kelkar, K. M. K., Karki, C., Tai, C., Lamb, C., and Patankar, S. V., "Numerical Prediction of Flow and Heat Transfer in an Impingement Heat Sink," Journal of Electronic Packaging, Vol. 119, No. 1, pp. 58-63, 1997.

[18] Jonsson, H. and Palm, B., "Thermal and Hydraulic Behavior of Plate Fin and Strip Fin Heat Sinks Under Varying Bypass Conditions," IEEE Transactions on Components and Packaging Technologies, Vol. 23, No. 1, pp. 47-54, 2000.

[19] Maveety, J. G. and Jung, H. H., "Design of an Optimal Pin-Fin Heat Sink with Air Impingement Cooling," International Communication on Heat and Mass Transfer, Vol. 27, No. 2, pp. 229-240, 2000.

[20] Chan,Y. T., Hu, A. G. C., and Plant, J. B., "A Kalman Filter Based Tracking Scheme with Input Estimation," IEEE Transactions on Aerospace and Electronic Systems, AES-15, pp. 237, 1979.